Internal Report IASF-BO 589/2011

Fitting ionization fraction and electron temperature histories for astrophysical reionization models

T. Trombetti[1,2] and C. Burigana[1,3]

[1] *INAF-IASF Bologna, Via P. Gobetti 101, I-40129, Bologna, Italy*
[2] *Dipartimento di Fisica, Università La Sapienza, P.le A. Moro 2, I-00185 Roma, Italy*
[3] *Dipartimento di Fisica, Università degli Studi di Ferrara, Via G. Saragat 1, I-44100 Ferrara, Italy*

Internal Report IASF-BO/589/2011

06/04/2011

Fitting ionization fraction and electron temperature histories for astrophysical reionization models

T. Trombetti[1,2] and C. Burigana[1,3]

[1]*INAF-IASF Bologna, via P. Gobetti 101, I-40129, Bologna, Italy*
[2]*Dipartimento di Fisica, Università La Sapienza, P.le A. Moro 2, I-00185 Roma, Italy*
[3]*Dipartimento di Fisica, Università degli Studi di Ferrara, Via G. Saragat 1, I-44100 Ferrara, Italy*

SUMMARY – The accurate understanding of the ionization history of the universe plays a fundamental role in the modern cosmology. The cosmological reionization leaves imprints on the CMB depending on the (coupled) ionization and thermal history. The inclusion of astrophysically motivated ionization and thermal histories in numerical codes is crucial for the accurate prediction of the features induced in the CMB, for constraining reionization models with CMB data, and to exploit current and future high quality CMB data with great versatility to extract their overall cosmological information. Having functional descriptions of evolution histories of the ionization fraction and thermal history allows to speed-up computation and improve versatility of existing codes with respect to the use of interpolation of tabulated grids. We describe the use of a tool able to find in a versatile way suitable functional representation of reionization histories and apply it to two well-based radiative feedback reionization models. The accuracy of the method is also discussed.

1 Introduction and theoretical framework

The accurate understanding of the ionization history of the universe plays a fundamental role in the modern cosmology. The classical theory of hydrogen recombination for pure baryonic cosmological models [26, 40] has been subsequently extended to non-baryonic dark matter models [39, 18, 31] and recently accurately updated to include also helium recombination in the current cosmological scenario (see [37] and references therein). Various models of the subsequent universe ionization history have been considered to take into account additional sources of photon and energy production, possibly associated to the early stages of structure and star formation, able to significantly increase the free electron fraction, x_e, above the residual fraction ($\sim 10^{-3}$) after the standard recombination epoch at $z_{\rm rec} \simeq 10^3$. These photon and energy production processes associated to this reionization phase may leave imprints in the cosmic microwave background (CMB) providing a crucial "integrated" information on the so-called *dark* and *dawn ages*, i.e. the epochs before or at the beginning the formation of first cosmological structures. For this reason, among the extraordinary results achieved by the *Wilkinson Microwave Anisotropy Probe* (WMAP) mission, the contribution to the understanding of the cosmological reionization process has received a great attention.

To first approximation, the beginning of the reionization process is identified by the Thomson optical depth, τ. The values of τ compatible with WMAP 3yr data, possibly complemented with external data, are typically in the range $\sim 0.06 - 0.12$ (corresponding to a reionization redshift in the range $\sim 8.5 - 13.5$ for a sudden reionization history), the exact interval depending on the considered cosmological model and combination of data sets [35]. While this simple "τ-parametrization" of the reionization process and, in particular, of its imprints on the CMB anisotropy likely represents a sufficiently accurate modelling for the interpretation of current CMB data, a great attention has been recently posed on the accurate computation of the reionization signatures in the CMB for a large variety of astrophysical scenarios and physical processes (see e.g. [27, 8, 4, 7, 9, 19, 16, 28, 38]) also in the view of WMAP accumulating data and of forthcoming and future experiments beyond WMAP (see [2] for a review). In [33] a detailed study of the impact of reionization, and the associated radiative feedback, on galaxy formation and of the corresponding detectable signatures has been presented, focussing on a detailed comparison of two well defined alternative prescriptions (*suppression* and *filtering*) for the radiative feedback mechanism suppressing star formation in small-mass halos, showing that they are consistent with a wide set of existing observational data but predict different 21 cm background signals accessible to future observations. The corresponding signatures detectable in the CMB have been then computed in [3].

1.1 Signatures in the CMB

The cosmological reionization leaves imprints on the CMB depending on the (coupled) ionization and thermal history. They can be divided in three categories[1]: *i*) generation of CMB Comptonization and free-free spectral distortions associated to the IGM electron temperature increase during the reionization epoch, *ii*) suppression of CMB temperature anisotropes at large multipoles, ℓ, due to photon diffusion, and *iii*) increasing of the power of CMB polarization and temperature-polarization cross-correlation anisotropy at various multipole ranges, mainly depending on the reionization epoch, because of the delay of the effective last scattering surface.

[1]Inhomogeneous reionization also produces CMB secondary anisotropies that dominate over the primary CMB component for $l \gtrsim 4000$ and can be detected by upcoming experiments, like the Atacama Cosmology Telescope or ALMA [30, 17].

The imprints on CMB anisotropies are mainly dependent on the ionization history while CMB spectral distortions strongly depend also on the thermal history.

Through this note we assume a flat ΛCDM cosmological model consistent with WMAP described by matter and cosmological constant (or dark energy) density parameters $\Omega_m = 0.24$ and $\Omega_\Lambda = 0.76$, reduced Hubble constant $h = H_0/(100\mathrm{km/s/Mpc}) = 0.73$, baryon density $\Omega_b h^2 = 0.022$, density contrast $\sigma_8 = 0.74$, and adiabatic scalar perturbations (without running) with spectral index $n_s = 0.95$. We assume a CMB background temperature of 2.725 K [23].

1.2 Reionization models

The latest analysis of Lyα absorption in the spectra of the 19 highest redshift Sloan Digital Sky Survey (SDSS) quasars (QSOs) shows a strong evolution of the Gunn-Peterson Lyα opacity at $z \sim 6$ [10, 12]. The downward revision of the electron scattering optical depth to $\tau = 0.09 \pm 0.03$ in the release of the 3yr WMAP data [25, 35], is consistent with "minimal reionization models" which do not require the presence of very massive ($M > 100 M_\odot$) Pop III stars [6, 14]. According to the 7yr WMAP analysis [21], the current uncertainty on τ is $\simeq \pm 0.015$, almost independently on the specific model considered. Under various hypotheses (simple ΛCDM model with six parameters, inclusion of curvature and dark energy, of different kinds of isocurvature modes, of neutrino properties, of primordial helium mass fraction, or of a re-ionization width) the best fit of τ lies in the range 0.086–0.089, while allowing for the presence of primordial tensor perturbations or (and) of a running in the power spectrum of primordial perturbations the best fit of τ goes to 0.091–0.092 (0.096). The above models can be then used to explore the effects of reionization on galaxy formation, referred to as "radiative feedback".

A semi-analytic model to jointly study cosmic reionization and the thermal history of the intergalactic medium (IGM) has been developed in [5, 6] . According to [33], the semi-analytical model developed by [5] complemented by the additional physics introduced in [6] involves: *i*) the treatment of IGM inhomogeneities by adopting the procedure of [24]; *ii*) the modelling of the IGM treated as a multiphase medium, following the thermal and ionization histories of neutral, HII, and HeIII regions simultaneously in the presence of ionizing photon sources represented by Pop III stars with a standard Salpeter IMF extending in the range $1 - 100\ M_\odot$ [32], Pop II stars with $Z = 0.2 Z_\odot$ and Salpeter IMF, and QSOs (particularly relevant at $z \lesssim 6$); *iii*) the chemical feedback controlling the prolonged transition from Pop III to Pop II stars in the merger-tree model by [32]; *iv*) assumptions on the escape fractions of ionizing photons, considered to be independent of the galaxy mass and redshift, but scaled to the amount of produced ionizing photons. It then accounts for radiative feedback inhibiting star formation in low-mass galaxies. This semi-analytical model is determined by only four free parameters: the star formation efficiencies of Pop II and Pop III stars, a parameter, $\eta_{\rm esc}$, related to the escape fraction of ionizing photons emitted by Pop II and Pop III stars, and the normalization of the photon mean free path, λ_0, set to reproduce low-redshift observations of Lyman-limit systems [5].

A variety of feedback mechanisms can suppress star formation in mini-halos, i.e. halos with virial temperatures $T_{vir} < 10^4$ K, particularly if their clustering is taken into account [20]. We therefore assume that stars can form in halos down to a virial temperature of 10^4 K, consistent with the interpretation of the 3yr WMAP data [15] (but see also [1]). Even galaxies with virial temperature $T_{vir} \gtrsim 10^4$ K can be significantly affected by radiative feedback during the reionization process, as the increase in temperature of the cosmic gas can dramatically suppress their formation. Based on cosmological simulations of reionization, [13] developed an accurate characterization of the radiative feedback on low-mass galaxies. This study shows

that the effect of photoionization is controlled by a single mass scale in both the linear and non-linear regimes. The gas fraction within dark matter halos at any given moment is fully specified by the current filtering mass, which directly corresponds to the length scale over which baryonic perturbations are smoothed in linear theory. The results of this study provide a quantitative description of radiative feedback, independently of whether this is physically associated to photoevaporative flows or due to accretion suppression.

Two specific alternative prescriptions for the radiative feedback by these halos have been considered [33, 3]:
i) *suppression model* – following [6], we assume that in photoionized regions halos can form stars *only* if their circular velocity exceeds the critical value $v_{\rm crit} = 2k_B T/\mu m_{\rm p}$; here μ is the mean molecular weight, $m_{\rm p}$ is the proton mass, and T is the average temperature of ionized regions, computed self-consistently from the multiphase IGM model;
ii) *filtering model* – following [13], we assume that the average baryonic mass M_b within halos in photoionized regions is a fraction of the universal value $f_b = \Omega_b/\Omega_m$, given by the fitting formula $M_b/M = f_b/[1 + (2^{1/3} - 1)M_{\rm C}/M]^3$, where M is the total halo mass and $M_{\rm C}$ is the total mass of halos that on average retain 50% of their gas mass. A good approximation for the characteristic mass $M_{\rm C}$ is given by the linear-theory filtering mass, $M_{\rm F}^{2/3} = (3/a)\int_0^a da' M_{\rm J}^{2/3}(a') \left[1 - (a'/a)^{1/2}\right]$, where a is the cosmic scale factor, $M_{\rm J} \equiv (4\pi/3)\bar{\rho}\left(\pi c_{\rm s}^2/G\bar{\rho}\right)^{3/2}$, is the Jeans mass, $\bar{\rho}$ is the average total mass density of the Universe, and $c_{\rm s}$ is the gas sound speed.

The model free parameters are constrained by a wide range of observational data. [33] reported the best fit choice of the above four parameters for these two models that well accomplish a wide set of astronomical observations, such as the redshift evolution of Lyman-limit absorption systems, the Gunn-Peterson and electron scattering optical depths, the cosmic star formation history, and number counts of high redshift sources in the NICMOS Hubble Ultra Deep Field.

The two feedback prescriptions have a noticeable impact on the overall reionization history and the relative contribution of different ionizing sources. In fact, although the two models predict similar global star formation histories dominated by Pop II stars, the Pop III star formation rates have markedly different redshift evolution. Chemical feedback forces Pop III stars to live preferentially in the smallest, quasi-unpolluted halos (virial temperature $\gtrsim 10^4$ K, [32]), which are those most affected by radiative feedback. In the suppression model, where star formation is totally suppressed below $v_{\rm crit}$, Pop III stars disappear at $z \sim 6$; conversely, in the filtering model, where halos suffer a gradual reduction of the available gas mass, Pop III stars continue to form at $z \lesssim 6$, though with a declining rate. Since the star formation and photoionization rate at these redshifts are observationally well constrained, the star formation efficiency and escape fraction of Pop III stars need to be lower in the filtering model in order to match the data. Therefore reionization starts at $z \lesssim 15$ in the filtering model and only 16% of the volume is reionized at $z = 10$ (while reionization starts at $z \sim 20$ in the suppression model and it is 85% complete by $z = 10$). For $6 < z < 7$, QSOs, Pop II and Pop III give a comparable contribution to the total photo-ionization rate in the filtering model, whereas in the suppression model reionization at $z < 7$ is driven primarily by QSOs, with a smaller contribution from Pop II stars only.

The predicted free electron fraction and gas temperature evolution in the redshift range $7 < z < 20$ is very different for the two feedback models. In particular, in the filtering model the gas kinetic temperature is heated above the CMB value only at $z \lesssim 15$.

The Thomson optical depth, $\tau = \int \chi_e n_e \sigma_T c dt$, can be directly computed for the assumed ΛCDM cosmological model parameters given the ionization histories: $\tau \simeq 0.1017$ and $\tau \simeq 0.0631$ for the suppression and the filtering model, respectively. Note that these values are

consistent with the Thomson optical depth range derived from WMAP 3yr (7yr) data but with $\sim 1\sigma$ ($\sim 2\sigma$) difference among the two models, leaving a chance of accurately probing them with forthcoming CMB anisotropy experiments.

1.3 Aim of this report

The inclusion of astrophysically motivated ionization and thermal histories in numerical codes for the prediction of the features induced in the CMB is crucial both for constraining reionization models with CMB data and to exploit current and future high quality CMB data with great versatility to extract their overall cosmological information. Since the accuracy achieved by COBE-FIRAS [11], a great precision in the computation of CMB spectral distortions [36, 41, 42] is required for a state-of-the-art analysis of absolute CMB temperature data. Current numerical codes for the solution of the Kompaneets equation in cosmological context [29] can ingest very general ionization and thermal histories. The above astrophysical reionization models, as well as many others published in the literature, typically provide these histories in tabulated form. The code in [29] is currently implemented to be able to ingest tables of reionization models for both temperature and ionization fraction and to (in linear or logarithmic space) interpolated over their grids, but it will be very useful to have functional descriptions of them in order speed-up computation and improve code versatility. The cosmological analysis of WMAP data and the forthcoming *Planck* data largely relies on Boltzmann codes [34, 22] for computing the CMB angular power spectrum in temperature, polarization, and cross-correlation modes under general conditions. The inclusion in such codes of reonization histories, namely the evolution of the ionization fraction, beyond the simplistic phenomenological approximations already implemented in the publicly available codes, allows to achieve more accurate prediction, of particular interest for the analysis of polarization data, as discussed for example in [3]. Again, having functional descriptions of evolution histories of the ionization fraction allows to speed-up computation and improve code versatility with respect to the use of interpolation of tabulated grids. In the following sections we will describe the use of a tool able to find in a versatile way suitable functional representation of reionization histories (Sect. 2) and will apply it to the two radiative feedback reionization models (*filtering* and *suppression*) described in previous sections, to arrive to their functional representation (Sects. 3 and 4). Then, we will evaluate the accuracy of the found representations (Sect. 5). Finally, we summarize our main results (Sect. 6).

2 Fit tool

The software used to produce the fit to the data is *Igor Pro v. 6.21* [43], an integrated program for visualizing, analyzing, transforming and presenting experimental data, such as curve-fitting, Fourier transforms, smoothing, statistics, and other data analysis, image display and processing, by a combination of graphical and command-line user interface.

The basic Igor's objects are *waves, graphs and tables*. A collection of object is called *experiment*, and stored in an experiment file. The wave is the object that contains the array of numbers, which can be shown in a table.

The *Page Layout* object display multiple graphs and tables, as well as pictures and annotations, for a presentation.

To apply Igor's operations and functions to new objects the user can follow three different ways, that are:
1) via menus and dialogs,
2) by typing Igor commands directly into the command line,

3) by writing Igor procedures.

The *command window* is Igor's control center. A red line divides the command line, at the bottom of the window, and the history area, in which are stored executed commands and results of data analysis, like curve fitting or wave statistics. The first step is to load the data from an external file into a table, and to do this the user needs to go to the *Data* menu item, then in *Load Waves* and finally in *Load General Text*. When the dialog box appears the user has the capability to specify the name of each column, its respective format, and he should also ensure to check the *Make Table* option. Once the data are loaded it is feasible to make a graph going in the *Windows* menu item and choosing *New Graph*. It will appear a new window in which it is possible to select the y versus x waves. To modify all the parameters of the axis, like the scale, the tick, the grid, double click directly on the axis to show the *Modify Axis* dialog box. It is also possible to add a legend or a tag to a plot by the corresponding *Add Annotation* menu item. At this point everything is ready for the curve fitting. The user can decide to take the entire dataset, or a subset of the data. Go to the *Graph* menu item and select the *Show Info* option, to visualize the *Cursor Info* panel to the bottom of the graph. Place *cursor A*, the round one, on the *fakeY* trace, the initial point of the interval, by dragging it on the corresponding point of the curve. Then place the *cursor B*, the square one, on the other interval's extreme. One way of fitting the data is represented by the *Quick Fit* option in the *Analysis* menu. The fit is evaluated only over the subrange identified by the cursors. Similarly, the user can choose the *Curve Fitting* option in the same menu and setup the right parameters.

3 Results: ionization fraction

3.1 Reionization in CF06

In this section we provide the fit functions for the reionization history CF06. Fig. 1 shows the comparison between the data and the fit of the ionization fraction.

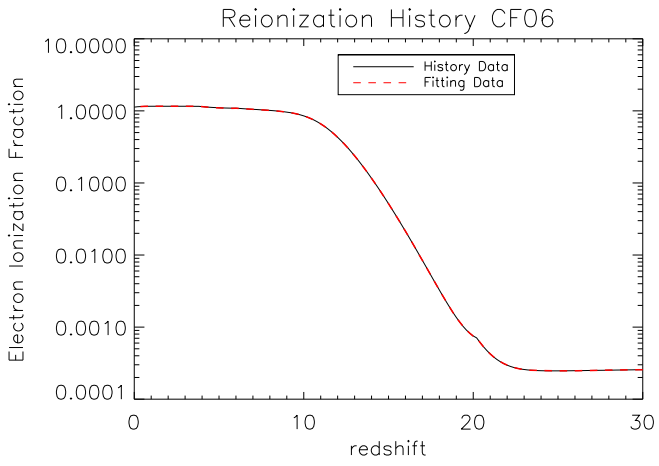

Figure 1: Ionization fraction: comparison between the data and the fit in the reionization history CF06.

- Interval $z = [0, 3.8]$ - Polinomial Function of 6° order:

$$a_0 = 1.12751$$

$$a_1 = 0.082246$$

$$a_2 = -0.083182$$

$$a_3 = 0.041472$$

$$a_4 = -0.010615$$

$$a_5 = 0.0012916$$

$$a_6 = -5.5608e-05$$

$$\chi_{re} = a_0 + a_1 z + a_2 z^2 + a_3 z^3 + a_4 z^4 + a_5 z^5 + a_6 z^6$$

- Interval $z = [3.8, 6]$ - Polinomial Function of 5° order:

$$b_0 = -14.708$$

$$b_1 = 16.69$$

$$b_2 = -6.8995$$

$$b_3 = 1.4055$$

$$b_4 = -0.14167$$

$$b_5 = 0.0056647$$

$$\chi_{re} = b_0 + b_1 z + b_2 z^2 + b_3 z^3 + b_4 z^4 + b_5 z^5$$

- Interval $z = [6, 9]$ - Polinomial Function of 5° order:

$$c_0 = -8.6358$$

$$c_1 = 6.7374$$

$$c_2 = -1.821$$

$$c_3 = 0.24108$$

$$c_4 = -0.015686$$

$$c_5 = 0.00040015$$

$$\chi_{re} = c_0 + c_1 z + c_2 z^2 + c_3 z^3 + c_4 z^4 + c_5 z^5$$

- Interval $z = [9, 12.4]$ - Log-Normal Function:

$$l_0 = 1.0061$$

$$l_1 = -0.83887$$

$$l_2 = 14.107$$

$$l_3 = 0.26413$$

$$\chi_{re} = l_0 + l_1 \exp\left[-\left(\frac{\ln(z/l_2)}{l_3}\right)^2\right]$$

- Interval $z = [12.4, 14.2]$ - Sigmoidal Function:

$$d_0 = 1.1468$$

$$d_1 = -1.153$$

$$d_2 = 11.39$$

$$d_3 = 1.2238$$

$$\chi_{re} = d_0 + \frac{d_1}{1 + \exp\left(\frac{d_2 - z}{d_3}\right)}$$

- Interval $z = [14.2, 16.8]$ - Hill Equation:

$$e_0 = -0.0021632$$

$$e_1 = 0.46249$$

$$e_2 = -13.862$$

$$e_3 = 12.952$$

$$\chi_{re} = e_0 + (e_1 - e_0)\frac{z^{e_2}}{z^{e_2} + e_3^{e_2}}$$

- Interval $z = [16.8, 18]$ - Decaying Exponential Function (expXOffset):

$$h_0 = 7.2284e - 06$$

$$h_1 = 0.010169$$

$$h_2 = 1.054$$

$$h_3 = 16.8$$

$$\chi_{re} = h_0 + h_1 \exp\left(\frac{h_3 - z}{h_2}\right)$$

- Interval $z = [18, 20]$ - Hill Equation:

$$i_0 = 0.00048712$$

$$i_1 = 0.013733$$

$$i_2 = -24.474$$

$$i_3 = 17.051$$

$$\chi_{re} = i_0 + (i_1 - i_0)\frac{z^{i_2}}{z^{i_2} + i_3^{i_2}}$$

- Interval $z = [20, 20.2]$ - Linear Function:

$$m_0 = 0.0052133$$

$$m_1 = -0.000223$$

$$\chi_{re} = m_0 + m_1 z$$

- Interval $z = [20.2, 23]$ - Decaying Exponential Function (expXOffset):

$$f_0 = 0.00023877$$

$$f_1 = 0.00047086$$

$$f_2 = 0.85918$$

$$f_3 = 20.2$$

$$\chi_{re} = f_0 + f_1 \exp\left(\frac{f_3 - z}{f_2}\right)$$

- Interval $z = [23, 30]$ - Log-Normal Function:

$$g_0 = 0.00025689$$

$$g_1 = -9.6891e - 06$$

$$g_2 = 25.421$$

$$g_3 = 0.10111$$

$$\chi_{re} = g_0 + g_1 \exp\left[-\left(\frac{\ln(z/g_2)}{g_3}\right)^2\right]$$

3.2 Reionization in G00

In this section we provide describe the fit functions for the reionization history G00. Fig. 2 shows the comparison between the data and the fit of the ionization fraction.

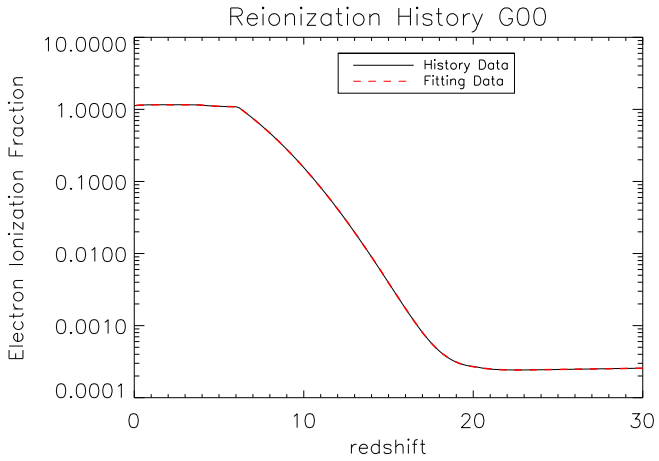

Figure 2: Ionization fraction: comparison between the data and the fit in the reionization history G00.

- Interval $z = [0, 3.8]$ - Polinomial Function of 9° order:

$$a_0 = 1.1245$$

$$a_1 = 0.10495$$

$$a_2 = -0.19535$$

$$a_3 = 0.25489$$

$$a_4 = -0.20598$$

$$a_5 = 0.098856$$

$$a_6 = -0.028032$$

$$a_7 = 0.0045895$$

$$a_8 = -0.00040036$$

$$a_9 = 1.4397e-05$$

$$\chi_{re} = a_0 + a_1 z + a_2 z^2 + a_3 z^3 + a_4 z^4 + a_5 z^5 + a_6 z^6 + a_7 z^7 + a_8 z^8 + a_9 z^9$$

- Interval $z = [3.8, 6]$ - Log-Normal Function:

$$i_0 = 1.8818$$

$$i_1 = -0.7941$$

$$i_2 = 6.3915$$

$$i_3 = 1.7469$$

$$\chi_{re} = i_0 + i_1 \exp\left[-\left(\frac{\ln(z/i_2)}{i_3}\right)^2\right]$$

- Interval $z = [6, 6.2]$ - Linear Function:

$$m_0 = 2.2768$$

$$m_1 = -0.1981$$

$$\chi_{re} = m_0 + m_1 z$$

- Interval $z = [6.2, 9]$ - Hill Equation:

$$l_0 = -0.1805$$

$$l_1 = 2.7323$$

$$l_2 = -3.6558$$

$$l_3 = 5.6876$$

$$\chi_{re} = l_0 + (l_1 - l_0)\frac{z^{l_2}}{z^{l_2} + l_3^{l_2}}$$

- Interval $z = [9, 11.6]$ - Sigmoidal Function:

$$b_0 = 1.1438$$

$$b_1 = -1.1441$$

$$b_2 = 7.3904$$

$$b_3 = 1.4126$$

$$\chi_{re} = b_0 + \frac{b_1}{1 + \exp\left(\frac{b_2 - z}{b_3}\right)}$$

- Interval $z = [11.6, 13]$ - Power Function:

$$c_0 = -0.0089383$$

$$c_1 = 2.0529e+06$$

$$c_2 = -7.0525$$

$$\chi_{re} = c_0 + c_1 z^{c_2}$$

- Interval $z = [13, 15]$ - Power Function:

$$h_0 = -0.0015104$$

$$h_1 = 9.1637e + 08$$

$$h_2 = -9.5468$$

$$\chi_{re} = h_0 + h_1 z^{h_2}$$

- Interval $z = [15, 17]$ - Decaying Exponential Function (expXOffset):

$$d_0 = 0.00013226$$

$$d_1 = 0.003812$$

$$d_2 = 1.1503$$

$$d_3 = 15$$

$$\chi_{re} = d_0 + d_1 \exp\left(\frac{d_3 - z}{d_2}\right)$$

- Interval $z = [17, 19.6]$ - Decaying Exponential Function (expXOffset):

$$e_0 = 0.00023759$$

$$e_1 = 0.00057014$$

$$e_2 = 0.98278$$

$$e_3 = 17$$

$$\chi_{re} = e_0 + e_1 \exp\left(\frac{e_3 - z}{e_2}\right)$$

- Interval $z = [19.6, 22.2]$ - Decaying Exponential Function (expXOffset):

$$f_0 = 0.00023514$$

$$f_1 = 4.6107e - 05$$

$$f_2 = 1.3061$$

$$f_3 = 19.6$$

$$\chi_{re} = f_0 + f_1 \exp\left(\frac{f_3 - z}{f_2}\right)$$

- Interval $z = [22.2, 30]$ - Decaying Exponential Function (expXOffset):

$$g_0 = 0.052228$$

$$g_1 = -0.051987$$

$$g_2 = 26607$$

$$g_3 = 22.2$$

$$\chi_{re} = g_0 + g_1 \exp\left(\frac{g_3 - z}{g_2}\right)$$

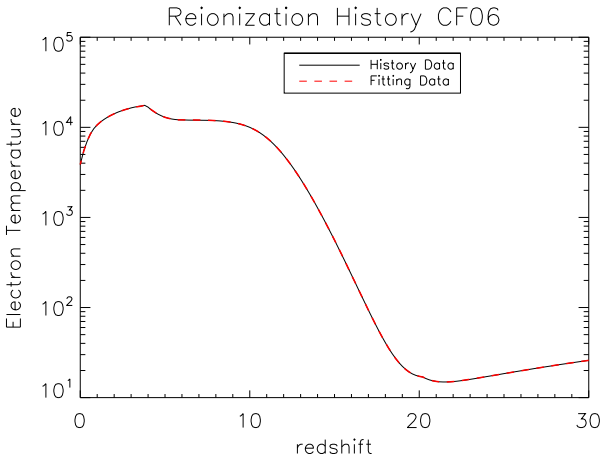

Figure 3: Electron temperature: comparison between the data and the fit in the reionization history CF06.

4 Results: electron temperature

4.1 Temperature in CF06

In this section we provide the fit functions for the electron temperature history CF06. Fig. 3 shows the comparison between the data and the fit of the electron temperature.

- Interval $z = [0, 3.8]$ - Polinomial Function of 8° order:

$$a_0 = 3870$$

$$a_1 = 6793.7$$

$$a_2 = 7221.8$$

$$a_3 = -15962$$

$$a_4 = 13644$$

$$a_5 = -6419.7$$

$$a_6 = 1734.7$$

$$a_7 = -252.65$$

$$a_8 = 15.379$$

$$T_{re} = a_0 + a_1 z + a_2 z^2 + a_3 z^3 + a_4 z^4 + a_5 z^5 + a_6 z^6 + a_7 z^7 + a_8 z^8$$

- Interval $z = [3.8, 5.8]$ - Sigmoidal Function:

$$b_0 = 20934$$

$$b_1 = -8982.3$$

$$b_2 = 4.0373$$

$$b_3 = 0.45319$$

$$T_{re} = b_0 + \frac{b_1}{1 + \exp\left(\frac{b_2 - z}{b_3}\right)}$$

- Interval $z = [5.8, 13]$ - Hill Equation:

$$c_0 = -204.2$$
$$c_1 = 12105$$
$$c_2 = -10.529$$
$$c_3 = 11.612$$
$$T_{re} = c_0 + (c_1 - c_0)\frac{z^{c_2}}{z^{c_2} + c_3^{c_2}}$$

- Interval $z = [13, 16]$ - Hill Equation:

$$l_0 = -60.289$$
$$l_1 = 8498.4$$
$$l_2 = -12.484$$
$$l_3 = 12.23$$
$$T_{re} = l_0 + (l_1 - l_0)\frac{z^{l_2}}{z^{l_2} + l_3^{l_2}}$$

- Interval $z = [16, 16.8]$ - Decaying Exponential Function (expXOffset):

$$d_0 = 0.78206$$
$$d_1 = 229.94$$
$$d_2 = 1.0994$$
$$d_3 = 16$$
$$T_{re} = d_0 + d_1 \exp\left(\frac{d_3 - z}{d_2}\right)$$

- Interval $z = [16.8, 18.6]$ - Hill Equation:

$$e_0 = 11.543$$
$$e_1 = 705.41$$
$$e_2 = -19.532$$
$$e_3 = 15.338$$
$$T_{re} = e_0 + (e_1 - e_0)\frac{z^{e_2}}{z^{e_2} + e_3^{e_2}}$$

- Interval $z = [18.6, 20.2]$ - Log-Normal Function:

$$h_0 = 16.488$$
$$h_1 = 34.915$$
$$h_2 = 17.003$$
$$h_3 = 0.082807$$
$$T_{re} = h_0 + h_1 \exp\left[-\left(\frac{\ln(z/h_2)}{h_3}\right)^2\right]$$

- Interval $z = [20.2, 21]$ - Sigmoidal Function:

$$i_0 = 23.26$$
$$i_1 = -8.5661$$
$$i_2 = 19.785$$
$$i_3 = 0.41168$$
$$T_{re} = i_0 + \frac{i_1}{1 + \exp\left(\frac{i_2 - z}{i_3}\right)}$$

- Interval $z = [21, 22]$ - Log-Normal Function:

$$g_0 = 15.453$$
$$g_1 = -0.54634$$
$$g_2 = 21.501$$
$$g_3 = 0.038693$$
$$T_{re} = g_0 + g_1 \exp\left[-\left(\frac{\ln(z/g_2)}{g_3}\right)^2\right]$$

- Interval $z = [22, 30]$ - Log-Normal Function:

$$f_0 = 60.399$$
$$f_1 = -46.863$$
$$f_2 = 18.997$$
$$f_3 = 0.82554$$
$$T_{re} = f_0 + f_1 \exp\left[-\left(\frac{\ln(z/f_2)}{f_3}\right)^2\right]$$

4.2 Temperature in G00

In this section we provide the fit functions for the electron temperature history G00. Fig. 4 shows the comparison between the data and the fit of the electron temperature.

- Interval $z = [0, 3.8]$ - Polinomial Function of 8° order:

$$a_0 = 3794.4$$
$$a_1 = 6241$$
$$a_2 = 8613.8$$
$$a_3 = -17286$$
$$a_4 = 14511$$
$$a_5 = -6902.3$$
$$a_6 = 1923.6$$
$$a_7 = -292.58$$
$$a_8 = 18.706$$

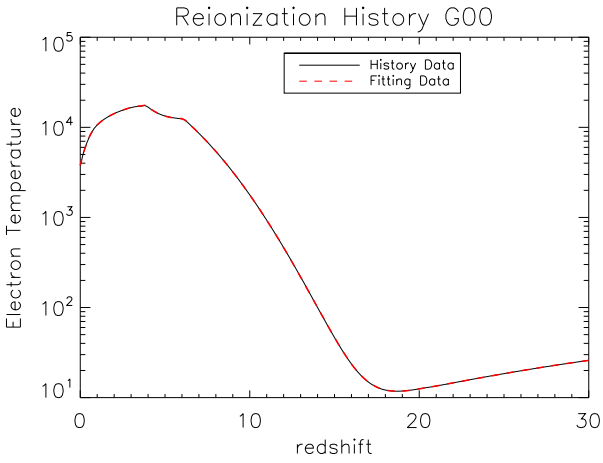

Figure 4: Electron temperature: comparison between the data and the fit in the reionization history CF06.

$$T_{re} = a_0 + a_1 z + a_2 z^2 + a_3 z^3 + a_4 z^4 + a_5 z^5 + a_6 z^6 + a_7 z^7 + a_8 z^8$$

- Interval $z = [3.8, 6.2]$ - Sigmoidal Function:

$$b_0 = 21591$$

$$b_1 = -9256.6$$

$$b_2 = 3.9293$$

$$b_3 = 0.50552$$

$$T_{re} = b_0 + \frac{b_1}{1 + \exp\left(\frac{b_2 - z}{b_3}\right)}$$

- Interval $z = [6.2, 10]$ - Log-Normal Function:

$$c_0 = 52588$$

$$c_1 = -51883$$

$$c_2 = 12.187$$

$$c_3 = 1.3666$$

$$T_{re} = c_0 + c_1 \exp\left[-\left(\frac{\ln(z/c_2)}{c_3}\right)^2\right]$$

- Interval $z = [10, 11]$ - Decaying Exponential Function (expXOffset):

$$h_0 = -210.57$$

$$h_1 = 1989.4$$

$$h_2 = 1.8033$$

$$h_3 = 10$$

$$T_{re} = h_0 + h_1 \exp\left(\frac{h_3 - z}{h_2}\right)$$

- Interval $z = [11, 15]$ - Sigmoidal Function:

$$d_0 = 4677.4$$
$$d_1 = -4674.2$$
$$d_2 = 9.2859$$
$$d_3 = 1.2229$$
$$T_{re} = d_0 + \frac{d_1}{1 + \exp\left(\frac{d_2 - z}{d_3}\right)}$$

- Interval $z = [15, 18]$ - Sigmoidal Function:

$$e_0 = 180.89$$
$$e_1 = -170.14$$
$$e_2 = 13.867$$
$$e_3 = 0.84978$$
$$T_{re} = e_0 + \frac{e_1}{1 + \exp\left(\frac{e_2 - z}{e_3}\right)}$$

- Interval $z = [18, 21]$ - Log-Normal Function:

$$f_0 = 14.387$$
$$f_1 = -2.5969$$
$$f_2 = 18.74$$
$$f_3 = 0.11421$$
$$T_{re} = f_0 + f_1 \exp\left[-\left(\frac{\ln(z/f_2)}{f_3}\right)^2\right]$$

- Interval $z = [21, 30]$ - Log-Normal Function:

$$g_0 = 8.1645$$
$$g_1 = 37.272$$
$$g_2 = 53.425$$
$$g_3 = 0.66903$$
$$T_{re} = g_0 + g_1 \exp\left[-\left(\frac{\ln(z/g_2)}{g_3}\right)^2\right]$$

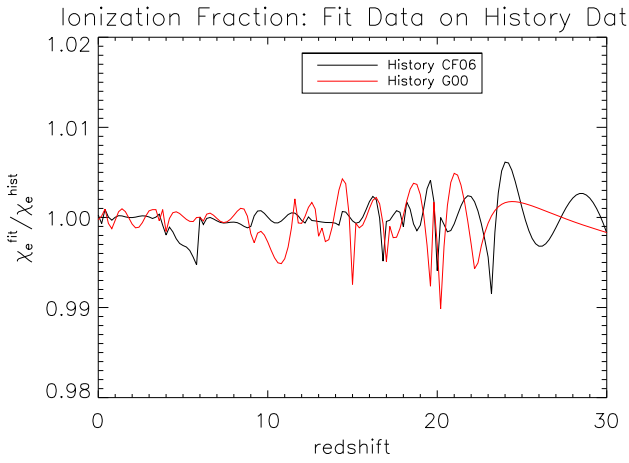

Figure 5: Ionization fraction: ratios between the fit functions and the data of the ionization fraction as function of the redshift for the two different reionization histories.

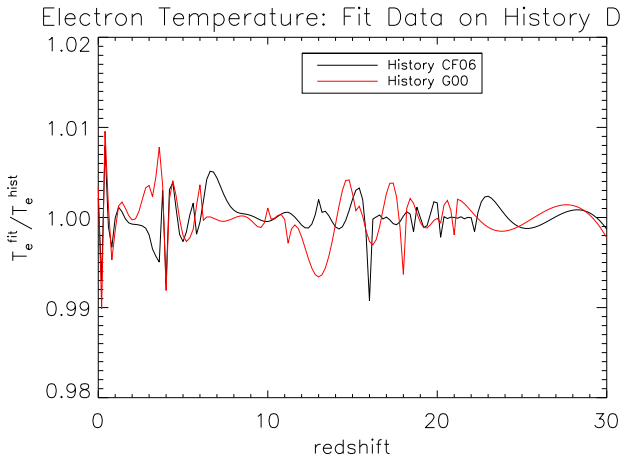

Figure 6: Electron temperature: ratios between the fit and the data of the electron temperature as function of the redshift for the two different reionization histories.

5 Accuracy of the fit functions

In this section we describe in details the accuracy of the fitting functions compared to the theoretical data.

By making the ratios between the two data arrays is possible to derive their percentile difference. In Fig. 5 are plotted the ratios between the fit functions and the data of the ionization fraction as function of redshift for the two different reionization histories. For both of them the difference is always $< 1\%$.

In the same way Fig. 6 shows the ratios between fit and theoretical data in the case of the electron temperature as function of redshift for the two different reionization histories. Again, for both of them, the difference is always $< 1\%$.

6 Conclusion

The accurate understanding of the ionization history of the universe plays a fundamental role in the modern cosmology. The cosmological reionization leaves imprints on the CMB depending on the (coupled) ionization and thermal history. The inclusion of astrophysically motivated ionization and thermal histories in numerical codes is crucial for the accurate prediction of the features induced in the CMB, for constraining reionization models with CMB data, and to exploit current and future high quality CMB data with great versatility to extract their overall cosmological information.

Having functional descriptions of evolution histories of the ionization fraction and thermal history allows to speed-up computation and improve versatility of existing codes with respect to the use of interpolation of tabulated grids.

We have described the use of a tool, the software *Igor Pro v. 6.21*, to find in a versatile way suitable functional representation of reionization histories. We have applied it to two well-based radiative feedback reionization models.

We found that, dividing the relevant redshift range in a set of suitable intervals, it is possible to find accurate functional representations of the considered reionization histories. The accuracy of the method is always better than 1% and typically less than few $\times$ 0.1%, making the found representations useful for many kinds of numerical applications, in the computation of both CMB spectral distortions and anisotropy angular power spectrum. The method can be easily applied to other reionization models.

Acknowledgements – It is a pleasure to thank T. Roy Choudhury, A. Ferrara, L.A. Popa, P. Procopio, R. Salvaterra, and R. Schneider for many constructive conversations on the cosmological reionization process.

References

[1] Alvarez M.A., Shapiro P.R., Ahn K., Iliev I.T., 2006, ApJ, 644, L101

[2] Burigana C., Finelli F., Salvaterra R., Popa L.A., Mandolesi N., 2004, Recent Res. Devel. Astronomy & Astrophys., Vol. 2(2004), p. 59

[3] Burigana C., Popa L.A., Salvaterra R., Schneider R., Choudhury T. Roy, Ferrara A., 2008, MNRAS, 385, 404

[4] Cen R., 2003, ApJ, 591, 12

[5] Choudhury T.R., Ferrara A., 2005, MNRAS, 361, 577

[6] Choudhury T.R., Ferrara A., 2006, MNRAS, 371, L55

[7] Ciardi B., Ferrara A., White S.M.D., 2003, MNRAS, 344, L7

[8] Doroshkevich A.G., Naselsky P.D., 2002, Phys. Rev. D, 65, 13517

[9] Doroshkevich A.G., Naselsky I.P., Naselsky P.D., Novikov I.D., 2002, ApJ, 586, 709

[10] Fan X. et al., 2006, AJ, 132, 117

[11] Fixsen D.J. et al., 1996, ApJ, 473, 576

[12] Gallerani S., Choudhury T.R., Ferrara A., 2006, MNRAS, 370, 1401

[13] Gnedin N., 2000, ApJ, 542, 535

[14] Gnedin N., Fan X., 2006, ApJ, 648, 1

[15] Haiman Z., Bryan G.L., 2006, ApJ, 650, 7

[16] Hansen S.H., Haiman Z., 2004, ApJ, 600, 26

[17] Iliev I.T., Pen U.-L., Bond J.R., Mellema G., Shapiro P.R., 2007, ApJ, 660, 933

[18] Jones B.J.T., Wyse R., 1985, A&A, 149, 144

[19] Kasuya S., Kawasaki M., Sugiyama N., 2004, Phys. Rev. D, 69, 023512

[20] Kramer R.H., Haiman Z., Oh S.P., 2006, ApJ, 649, 570

[21] Larson D. et. al., 2011, ApJS, 192, 16

[22] Lewis A., Challinor A., Lasenby A., 2000, ApJ, 538, 473

[23] Mather J.C., Fixsen D.J., Shafer R.A., Mosier C., Wilkinson D.T., 1999, ApJ, 512, 511

[24] Miralda-Escudé J., Haehnelt M., Rees M.J., 2000, ApJ, 530, 1

[25] Page L. et al., 2007, ApJS, 170, 335

[26] Peebles P.J.E., 1968, ApJ, 153, 1

[27] Peebles P.J.E., Seager S., Hu W., 2000, ApJ, 539, L1

[28] Popa L.A., Burigana C., Mandolesi N., 2005, NA, 11, 173

[29] Procopio P., Burigana C., 2009, A&A, 507, 1243

[30] Salvaterra R., Ciardi B., Ferrara A., Baccigalupi C., 2005, MNRAS, 360, 1063

[31] Seager S., Sasselov D.D., Scott D., 2000, ApJS, 128, 407

[32] Schneider R., Salvaterra R., Ferrara A., Ciardi B., 2006, MNRAS, 369, 825

[33] Schneider R., Salvaterra R., Choudhury T.R., Ferrara A., Burigana C., Popa L.A., 2008, MNRAS, 384, 1525

[34] Seljak U., Zaldarriaga M., 1996, ApJ, 469, 437

[35] Spergel D.N. et al., 2007, ApJS, 170, 377

[36] Sunyaev R.A., Zel'dovich Ya.B., 1970, Ap&SS, 7, 20

[37] Switzer E.R., Hirata C.M., 2008, Phys. Rev. D 77, 083008

[38] Wyithe J.S.B., Cen R., 2007, ApJ, 659, 890

[39] Zabotin N.A., Naselsky P.D., 1982, Sov. Astron., 26, 272

[40] Zel'dovich Ya. B., Kurt V., Sunyaev R.A., 1968, Zh. Eksp. Theor. Phys., 55, 278

[41] Zel'dovich Ya.B., Illarionov A.F., Sunyaev R.A., 1972, Zh. Eksp. Teor. Fiz., 62, 1216 [Sov. Phys. JEPT, 35, 643]

[42] Zel'dovich Ya.B., Sunyaev R.A., 1969, Ap&SS, 4, 301

[43] WaveMetrics Inc. 2010, Igor Pro (version 6.2)